Cohesive energy and interaction of superparamagnetic aggregates

N. Rojas, M. Cerda, A. Ravasio, and T. Rudge

COLLECTIONS

Paper published as part of the special topic on Chemical Physics, Energy, Fluids and Plasmas, Materials Science and Mathematical Physics

View Online   Export Citation   CrossMark

ARTICLES YOU MAY BE INTERESTED IN

Origin of band inversion in topological Bi_2Se_3
AIP Advances **10**, 095018 (2020); https://doi.org/10.1063/5.0022525

Enhancement of spin signals by thermal annealing in silicon-based lateral spin valves
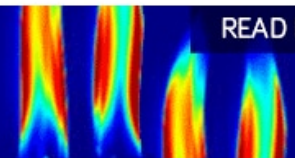AIP Advances **10**, 095021 (2020); https://doi.org/10.1063/5.0022160

Non-centric cavity-based acoustic metasurface: Enabling full phase modulation
AIP Advances **10**, 095020 (2020); https://doi.org/10.1063/5.0015662

Cohesive energy and interaction of superparamagnetic aggregates

View Online   Export Citation   CrossMark

N. Rojas,[1,a)] 🆔 M. Cerda,[1] A. Ravasio,[2] and T. Rudge[2,3]

AFFILIATIONS

[1] Anatomy and Developmental Biology Program, Institute of Biomedical Sciences, Faculty of Medicine, Universidad de Chile, P.O. Box 70031, Santiago, Chile

[2] Institute for Biological and Medical Engineering, Schools of Engineering, Biology and Medicine, Pontificia Universidad Católica de Chile, Santiago, Chile

[3] Department of Chemical and Bioprocess Engineering, School of Engineering, Pontificia Universidad Católica de Chile, Santiago, Chile

[a)] Author to whom correspondence should be addressed: nicolas.rojas@email.com

ABSTRACT

The self-assembly of monomers, chains, and bundles is often observed in magnetic mixtures. The most probable interaction between the aggregates in a superparamagnetic colloidal suspension is associated with the minimum of the effective magnetic potential in the two and three dimensional relative shift space, which yields a concrete criterion to be employed for prediction of the cohesive energy and the mean length of the aggregates in the fluid bulk.

I. INTRODUCTION

Understanding the physical bases of soft and hard speck coalescence is relevant in a great number of research fields ranging from embryonic development, nanotechnology, and material science. In particular, the use of magnetic colloidal particle dispersions (specifically, superparamagnetic colloids) is of fundamental importance in biomedical applications. Examples include capture of heavy metal pollutants in water, capture of microalgae in biofuels, microfluidics, and controlled protein assays.[1–3] The aggregation of magnetic colloids is a highly complex process, involving fundamental aspects of self-organization in magnetism and hydrodynamics. On the theoretical side, magnetic suspensions present a challenge in equilibrium thermodynamics, out-of-equilibrium physics (self-organization under equilibrium and non-equilibrium conditions), and fluid mechanics (lubrication, contact mechanics, convection induced by magnetism, and turbulence). Recognition of the importance of self-organization in this applied field has taken a lot of effort. Pioneering simulation works[4] have shown that chains break up and recombine in numerical runs. The latter is also ubiquitous

in experiments (see, for instance, Ref. 5). These initial results clearly indicate the existence of a rich and complex behavior, understanding of which would enable prediction and design of experiments and applications.

Superparamagnetic colloids are single-domain beads with a uniform magnetic moment.[6] In presence of a magnetic field $\vec{B}$, the particles self-assemble in chain-like structures. Chains interact building one-layered aggregates due to the screening inherited from the magnetic potential of interaction between two superparamagnetic particles,

$$U(r,\theta) = 4\varepsilon_m \frac{(1 - 3\cos^2\theta)}{(r/R)^3},\tag{1}$$

where $\varepsilon_m = \pi\chi^2 R^3 B^2/9\mu_0$; thus, the term *bundle* or *ribbon* in this work refers to one-layered clusters. The monomers are considered spheres of a mean radius R, θ is the relative angle between the line connecting the two beads and $\vec{B}$, with r being the distance between them. The cohesion energy of a dimer ε_m contains the magnetic susceptibility χ and the vacuum permeability μ_0. Sedimentation and

hydrodynamic forces are neglected, i.e., magnetic forces are considered dominant in the aggregation process (see more details about this assumption in Sec. IV). Researchers demonstrated explicitly the presence of self-organization and cooperative effects[7] related to the assembly of magnetic particles into moving chains and wider structures. In general, the magnetic potential of interaction (1) can be written by employing Cm^2/r^3, with C being a constant that depends on the type of magnetic grains in the suspension and m being the magnitude of the magnetic moment of the particles. These colloidal suspensions can be driven out of equilibrium by applying a regular magnet at one side of the vessel. The coupling between hydrodynamics and magnetism[8–10] induces convective effects and turbulence in heterogeneous magnetic field gradients, a process known as magnetophoresis, an essential step in all applications of magnetic colloids. With uniform magnetic fields applied (negligible gradients) and high values of intensity, chains and bundles grow up to a saturation regime where chains frequently clip off and migrate from the aggregates to join other bundles, and this exchange process is performed in thermodynamic equilibrium.[5]

In the latter regime, the mean length of the aggregates in the suspension remains roughly constant. In order to predict the dynamics of the coalescence process, there have been numerous previous simulation efforts, see, for instance, Ref. 11 for generic coalescence methods and scaling laws, Ref. 12 for ferromagnetic agglomeration under magnetic fields, Ref. 13 for dielectric particles under electric fields and chain formation of superparamagnetic beads,[14] Ref. 15 for superparamagnetic aggregation, and recent numerical findings where the magnetic saturation range was achieved.[16,17] The latter references provide full understanding of the aggregation of superparamagnetic grains into chains; hence, the prediction of ribbon coalescence and saturation processes will be carried out in a future work. The length of each chain n in the ribbons and their width d are nondimensional measures, normalized with the average grain diameter $2R$. The maximum width of the ribbons observed in experimental realizations is $d_{max} = 4$. These experiments were performed in a quasi-two-dimensional vessel. In practice, the width of the bundles is smaller than d due to compact packing; hence, d denotes only the number of chains assembled in a ribbon aligned parallel to $\vec{B}$, forming a single-layered aggregate. In a previous research study,[18] the relative displacement δ between two like sized chains in an aggregate was studied, and $\delta = 2$ was found to be the most favourable configuration. Nevertheless, for like sized chains at $d = 3, 4$ and for unlike sized chains at $d = 2, 3, 4$, the most plausible arrangements are unknown.

The goal of this contribution is to establish criteria and appropriate assumptions to compute and fit the magnetic energy per particle U_d in bundles formed by like sized and unlike sized chains. This is employed, for instance, to compute and predict the mean length of the aggregates in a colloidal mixture[19] as a function of magnetic field. In the latter work, aggregates formed by equally sized chains and relative displacements $\delta_i = 0$ (at odd i) and $\delta_j = -1$ (at even j) were assumed, whereas in Ref. 20, bundles formed by like sized chains and II-zig-zag cases (see also Sec. II B 1) formed by chains of length n and $n/2$ at relative shifts $\delta_i^{II} = 0$ (at odd i) and $\delta_j^{II} = -1$ (at even j) were considered to fit U_d. This arbitrariness on the parallel shifts (see definitions further in the text) considered to compute and fit U_d for each case $d = 2, 3, 4$ is solved by employing the highest ratio

between the configurations associated with the minima of U_d and the total number of possible interactions between unlike sized chains n_{max}^d (the number of chain size combinations in irregular bundles of a maximum chain length n_{max}), for each set of relative displacements $(\delta_1, \ldots, \delta_{d-1})$. The results in this work are focused on determining the most probable configurations in terms of the shifts between consecutive chains. The findings concern the relative displacements between chains in the directions parallel to the magnetic field at each junction, yielding sets of coordinates similar to those frequently encountered in crystallography. The paper is organized as follows: in Sec. II, ribbons formed by like sized chains of length n (regular bundles) are considered; in Sec. III irregular bundles with chains of maximum length allowed n_{max} are studied. The criteria found for computing the magnetic energy per particle of the agglomerates are employed to compute the mean length of the bundles in the magnetic suspension, which is compared upon experimental data[19] in Sec. IV. Conclusions are given in Sec. V.

II. LIKE SIZED CHAINS

In this section, regular aggregates formed by chains of equal size (the number of particles per chain) n are considered to search for the most plausible aggregate of width $d = 2, 3, 4$ in the colloidal blend. The total number of particles per agglomerate is $n_r = dn$. The cohesive energy of a dimer oriented parallel to $\vec{B}$ is ε_m. The magnetic energies are normalized with $\varepsilon_m/2$. The cohesion magnetic energy of a chain is $U_n^c = -2\sum_{i=1}^{n-1} \frac{n-i}{i^3}$.[18] The interaction energy between two chains is

$$U_n^{cc}(\delta_\parallel, \delta_\perp) = \sum_{i=1}^{n}\sum_{j=1}^{n}\left(\frac{1}{((j-i+\delta_\parallel)^2 + \delta_\perp^2)^{3/2}} - \frac{3(j-i+\delta_\parallel)^2}{((j-i+\delta_\parallel)^2 + \delta_\perp^2)^{5/2}}\right), \quad (2)$$

where $\delta_\parallel = 1/2 + \delta$ and $\delta_\perp = \sqrt{3}/2$ are the relative parallel and perpendicular (to the magnetic field) displacements between two assembled chains, respectively. These distances consider compact packing and integer values of δ (see Fig. 1). At $d = 2$, negative values of δ represent equivalent aggregates under reflection at the symmetric axis perpendicular to $\vec{B}$ having the same cohesive energy. Equation (2) presents the interaction potential between two chains, and this energy depends only on relative displacements since it has been length-chain averaged, as explained in Ref. 18. Therefore, the following magnetic potentials computed for 2-, 3-, and 4-chain bundles also depend on consecutive, interspersed, and lateral displacements. In this work, the term *interspersed* refers to being interspersed by a chain. The effective potential of a chain or a ribbon is angular dependent with attractive and repulsive regions due to screening, which allows the particles to aggregate only on the poles of chains, forming one-layered planes, as explained in Refs. 15 and 21. In the case of consecutive chains, $U_n^{cc}(\delta) = U_n^{cc}(1/2 + \delta, \sqrt{3}/2)$. The normalized cohesive energy per particle of a 2-chain aggregate is computed by employing U_n^c and $U_n^{cc}(\delta)$; then, $U_2(n,\delta) = [2U_n^c + U_n^{cc}(\delta)]/2n$. The cohesion energy of a 3-chain ribbon is also computed by employing U_n^c and $U_n^{cc}(\delta)$, in addition to the interaction energy between interspersed chains (in this case, these are the lateral chains of the bundle), which is obtained from (2) with $\delta_\parallel = \delta$ and $\delta_\perp = \sqrt{3}$, i.e.,
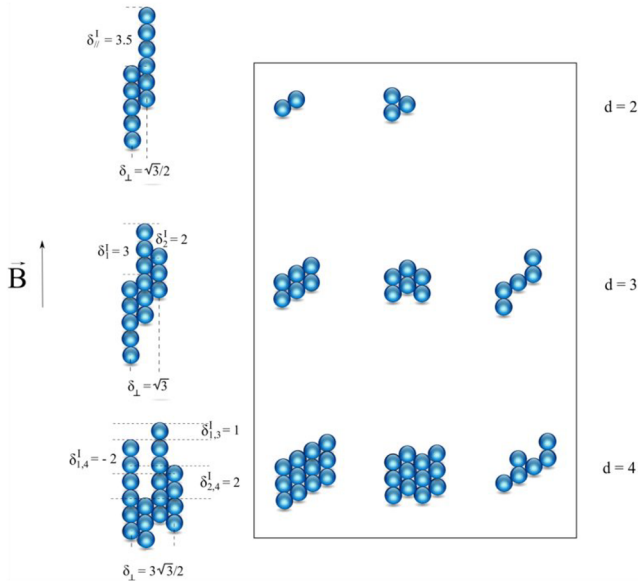
FIG. 1. Scheme displaying parallel, perpendicular displacements and consecutive, interspersed, and lateral shifts. Inset: examples of nonphysical regular and irregular aggregates at d = 2, 3, 4. The trimer at d = 2 occurs with small probability in experiments.

FIG. 2. Total reduced energy per particle U_2 of two like sized assembled chains as a function of the lateral relative displacement δ at n = 6 (dotted), n = 10 (dashed), and n = 25 (continuous) curves. The 2-chain regular aggregate at δ = 2 is schemed.

$U_n^{int}(\delta) = U_n^{cc}(\delta, \sqrt{3})$. Then, the normalized cohesive energy per particle of a 3-chain bundle is

$$U_3(n, \delta_{i,j}) = \frac{1}{3n}\left(3U_n^c + \sum_{i=1}^{2} U_n^{cc}(\delta_{i,i+1}) + U_n^{int}(\delta_{1,3})\right), \qquad (3)$$

with $\delta_{i,j}$ being the parallel displacement between chains i and j. It will be shown in Sec. II A that U_3 depends only on the lateral displacements between consecutive chains. The magnetic energy of a 4-chain aggregate is computed by employing U_n^c, $U_n^{cc}(\delta)$, $U_n^{int}(\delta)$, and the interaction energy between the first and fourth chains (external chains) $U_n^{ext}(\delta) = U_n^{cc}(1/2+\delta, 3\sqrt{3}/2)$. The normalized cohesive energy per particle of a 4-chain bundle is

$$U_4(n, \delta_{i,j}) = \frac{1}{4n}\left(4U_n^c + \sum_{i=1}^{3} U_n^{cc}(\delta_{i,i+1}) + \sum_{i=1}^{2} U_n^{int}(\delta_{i,i+2}) + U_n^{ext}(\delta_{1,4})\right). \qquad (4)$$

It will be shown in Sec. II B that U_4 depends only on consecutive lateral displacements. There are arrangements that represent nonphysical configurations, i.e., the probability to observe these aggregates in the colloidal mixture is very small (see examples in Fig. 1). These cases are negligible as $n \to \infty$ since the total number of interactions is higher than $(n-1)^{d-1}$.

A. 2- and 3-chain bundles

The results presented in Fig. 2 are in agreement with previous calculations,[18] where the most probable configurations are found at $\delta = -3$ and $\delta = 2$; these are defined as scale aggregates (see Table I).
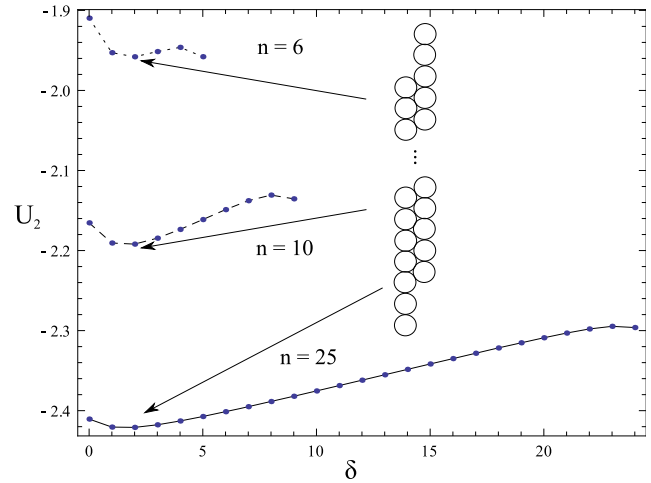
In general, the minima of the cohesion energy are found at equivalent configurations with equal energy (see Table II), and this is also supported by symmetry arguments. For three assembled chains forming a hexagonal lattice, the parallel displacements are assumed as $\delta_{\parallel} = 0(1/2) + \delta_{i,j}$ between interspersed (in contact) chains. For consecutive chains, $\delta_{1,2} \equiv \delta_1$ and $\delta_{2,3} \equiv \delta_2$.

There are two general cases of assembly: (δ_1, δ_2) of opposite signs (zig-zag bundles), side tails pointing to the same direction, and (δ_1, δ_2) both being positive or negative (scale aggregates), i.e., side tails pointing to opposite directions. The parallel displacement between the first and the third chain is $\delta_{1,3} = \delta_1 + \delta_2 + 1$. The latter confirms that the cohesion energy U_3 depends only on δ_1 and δ_2. In both cases, the minima of the cohesion energy U_3 (see Fig. 3) are searched numerically. In the former case (zig-zag bundles, see Tables I and II), the minima of U_3^{zig} are found at $(\delta_1, \delta_2) = (1, -6)$, $(\delta_1, \delta_2) = (-6, 1)$, $(\delta_1, \delta_2) = (5, -2)$, and $(\delta_1, \delta_2) = (-2, 5)$ for $n = 6$ and at $(\delta_1, \delta_2) = (1, -4)$, $(\delta_1, \delta_2) = (-4, 1)$, $(\delta_1, \delta_2) = (3, -2)$, and $(\delta_1, \delta_2) = (-2, 3)$ for $n \geq 10$ [see Fig. 3(a)], with lateral displacements $\delta_{1,3} = -2$ and $\delta_{1,3} = 2$, respectively.

For scale ribbons, the most probable configurations at $n = 6$ are $(\delta_1, \delta_2) = (-4, -3)$, $(\delta_1, \delta_2) = (-3, -4)$, $(\delta_1, \delta_2) = (2, 3)$, and $(\delta_1, \delta_2) = (3, 2)$, relative to 3 chains assembled with lateral chains pointing in opposite directions [see Fig. 3(b)]. For $n = 10$ and higher, the minima of each curve converge to $(\delta_1, \delta_2) = (-3, -3)$ and $(\delta_1, \delta_2) = (2, 2)$. These solutions represent the scale cases having $\delta_{1,3} = -5$ and $\delta_{1,3} = 5$, respectively, related to the global minima of U_3.

1. Discussion

Comparing aggregates with lateral tails in the same and opposite direction up to $n = 30$, one observes $|U_3^{sca}| > |U_3^{zig}|$ (see Table II), with $|U_3^{sca}|$ being the magnitude of the cohesion energy of aggregates with lateral tails pointing in opposite directions, i.e., scale aggregates with configurations $(\delta_1, \delta_2) = (-3, -3)$ and $(\delta_1, \delta_2) = (2, 2)$ are more likely to occur than zig-zag ribbons with

TABLE I. Consecutive parallel displacements δ_i in regular clusters at d = 2, 3, 4 as n increases (convergence arrangements). The signs indicate $\delta_i \geq 0$ (or $\delta_i < 0$) and $i = 1, \ldots, d-1$ in general configurations.

d	δ_i	Zig-zag-1	Zig-zag-2	Scale-1	Scale-2	Hill-1	Valley-1	Hill-2	Valley-2
2	δ			2	-3				
3	δ_1	$3\,\vert\,1$	$-2\,\vert\,-4$	2	-3				
	δ_2	$-2\,\vert\,-4$	$3\,\vert\,1$	2	-3				
4	δ_1	3	-4	2	-3	2	-3	1	-2
	δ_2	-2	1	2	-3	4	-5	-5	4
	δ_3	3	-4	2	-3	-2	1	-3	2

configurations associated with the minima of U_3^{zig} at $d = 3$. In order to verify that these arrangements are the ground states of 3 assembled chains of equal length n each, the energies of the states with parallel displacements δ_i, $\delta_i - 1$, and $i = 1, 2$ are considered to compute the differences,

$$\begin{aligned}\Delta U_{31}^{sca} &= U_3^{sca}(\delta_1, \delta_2) - U_3^{sca}(\delta_1 - 1, \delta_2) \\ \Delta U_{32}^{sca} &= U_3^{sca}(\delta_1, \delta_2) - U_3^{sca}(\delta_1, \delta_2 - 1)\end{aligned} \tag{5}$$

and the magnetic forces per particle in the aggregate,

$$\vec{F}_3^{sca} = -\nabla U_3^{sca} = -(\Delta U_{31}^{sca}\hat{\delta}_1 + \Delta U_{32}^{sca}\hat{\delta}_2), \tag{6}$$

for each coordinate parallel to the magnetic field. These are the effective forces at each junction, also considering the interaction between interspersed chains. Equation (6) is the backward difference scheme with a step $\Delta\delta_i = 1$ due to the depletion zone[22] at consecutive chains. The circle in Fig. 4 indicates the integer position $(\delta_1, \delta_2) = (2, 2)$ relative to the minimum of the magnetic potential encountered at $U_3^{sca(1)} < 0$. Notice in Fig. 4 that an integer shift in the positive (negative) direction of δ_i results in $F_{3i}^{sca(1)} < 0$ ($F_{3i}^{sca(1)} > 0$), i.e., the minimum is stable in δ_1 and δ_2; the latter is numerically verified also at $n = 50$ and $n = 100$. Computation of the minima for a higher number of particles can be achieved with the present method. The minimum of $U_3^{sca(1)}$ is found at a non-integer position; thus, $(\delta_1, \delta_2) = (2, 2)$ is the nearest integer pair [see Fig. 4(inset)]. Although this is not exactly the minimum of $U_3^{sca(1)}$, the aggregates remain in this configuration due to contact forces. In terms of the cohesive forces $\vec{F}_3^{sca(1)}$ in the coordinates parallel to the magnetic field at each junction, these are weakly repulsive at $(\delta_1, \delta_2) = (2, 2)$ and attractive toward this point at any other integer position as $n \to \infty$. Since the gradients of $U_3^{sca(1)}$ are computed for discrete values of δ_i,

the field lines are not perpendicular to every $U_3^{sca(1)}$ equipotential; thus, the force field is well defined only at integer values of the parameter space (δ_1, δ_2).

B. 4-chain aggregates

Bundles made of 4 chains have different shapes. Here, the possible configurations are classified into 3 groups: zig-zag, scale, and hill/valley aggregates (see Fig. 5). The lateral displacements of four assembled chains are given by $\delta_\parallel = (0)1/2 + \delta_{i,j}$ for (interspersed) consecutive or side chains. The perpendicular displacements are $\delta_\perp = \sqrt{3}/2$, $\sqrt{3}$, and $3\sqrt{3}/2$ for consecutive, interspersed, and external chains, respectively. Although it is possible to plot the magnetic potential of the aggregates, it is more difficult to visualize a possible minimum since the cohesion magnetic energy U_4 depends on 3 lateral displacements. The minima of U_4 for cases $n = 6, 10, 25, 30$ are computed numerically. The relative displacements in regions $l = I, II$ are equal, $\delta_{i,j}^I = \delta_{i,j}^{II}$ [see Fig. 5(a)].

1. Zig-zag ribbons

In the zig-zag configuration, the lateral displacements between interspersed chains are $\delta_{1,3}^l = \delta_1^l + \delta_2^l + 1$ and $\delta_{2,4}^l = \delta_2^l + \delta_3^l + 1$ and that between external chains is $\delta_{1,4}^l = \delta_1^l + \delta_2^l + \delta_3^l + 1$. The latter confirms that the cohesion energy U_4^{zig} of an assembled bundle depends only on the consecutive displacements δ_1^l, δ_2^l, and δ_3^l. For interspersed chains, it is assumed that $\delta_{i,i+2}^l = \delta_i^l + \delta_{i+1}^l + 1$ with $i = 1, 2$. The superscripts I, II are henceforth dropped, and only region I will be considered for the sake of simplicity. In the case $n = 6$, the minima of the normalized magnetic energy per particle U_4^{zig} are encountered at $(\delta_1, \delta_2, \delta_3) = (5, -2, 5)$ and $(\delta_1, \delta_2, \delta_3) = (-6, 1, -6)$ with the same

TABLE II. Minima of the cohesive magnetic energy per particle U_d in regular clusters at d = 1, 2, 3, 4 up to n = 30. At $d \geq 2$, each column represents two repeated values of the potential. The last column shows four repeated values of the potential per line.

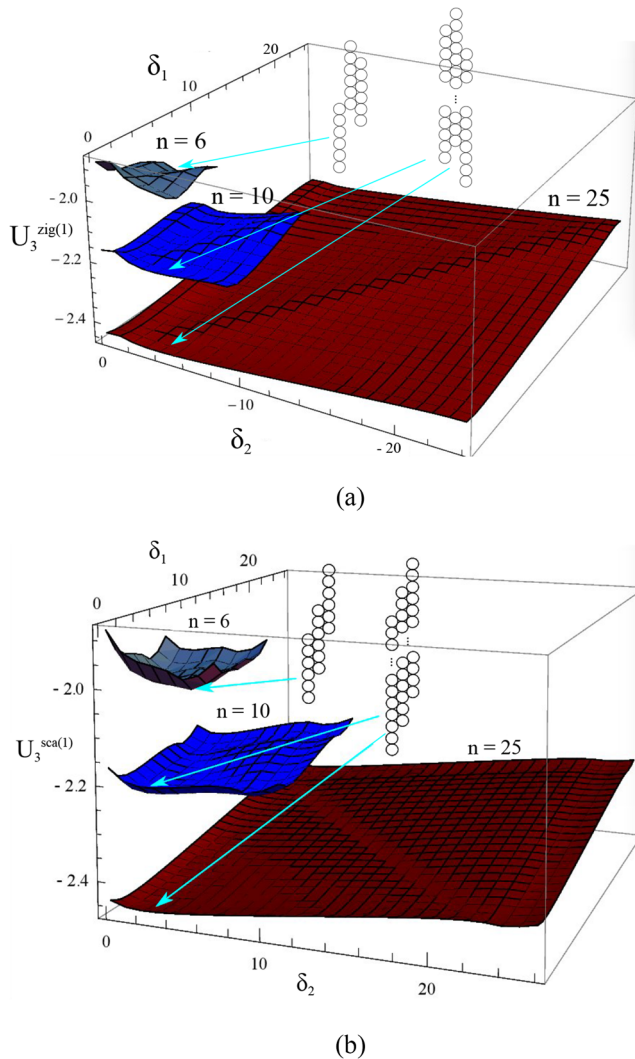| n	U_1	$U_2^{(1,2)}$	$U_3^{zig(1,2)}$	$U_3^{sca(1,2)}$	$U_4^{zig(1,2)}$	$U_4^{sca(1,2)}$	$U_4^{hil/val(1,2)}$
6	$-1.883\,45$	$-1.957\,94$	$-1.980\,14$	$-1.998\,46$	$-1.991\,5$	$-2.026\,96$	-2.009
10	$-2.085\,11$	$-2.191\,95$	$-2.203\,25$	$-2.223\,31$	$-2.222\,5$	$-2.245\,84$	$-2.235\,31$
25	$-2.274\,12$	$-2.420\,9$	$-2.458\,15$	$-2.465\,62$	$-2.474\,53$	$-2.486\,33$	$-2.480\,38$
30	$-2.295\,56$	$-2.447\,28$	$-2.487\,91$	$-2.494\,12$	$-2.506\,23$	$-2.516\,04$	$-2.511\,08$

(a)

(b)

FIG. 3. Total reduced energy per particle U_3 of three assembled chains at $n = 6$ (gray), $n = 10$ (blue), and $n = 25$ (red) surfaces for (a) zig-zag-1 aggregates, $\delta_1 \geq 0$ and $\delta_2 < 0$ and (b) scale-1 bundles, $\delta_1 \geq 0$ and $\delta_2 \geq 0$. Inset: schemed aggregates at one of the minima of each surface: (a) $(\delta_1, \delta_2) = (5, -2)$ at $n = 6$ and $(\delta_1, \delta_2) = (1, -4)$ at $n \geq 10$ and (b) $(\delta_1, \delta_2) = (2, 3)$ at $n = 6$ and $(\delta_1, \delta_2) = (2, 2)$ at $n \geq 10$.

energy, and this result corresponds to a pair of chains assembled to one chain at each side pointing to opposite directions. At $n = 10$, the most plausible configurations of a fully assembled bundle occurs at $(\delta_1, \delta_2, \delta_3) = (1, -10, 1)$ and $(\delta_1, \delta_2, \delta_3) = (-2, 9, -2)$, corresponding to two pairs of assembled chains pointing to opposite directions. At $n \geq 15$, the minima of U_3^{zig} are found at $(\delta_1, \delta_2, \delta_3) = (3, -2, 3)$ and $(\delta_1, \delta_2, \delta_3) = (-4, 1, -4)$, as schemed in Fig. 5(b); the latter result is also obtained with increasing n, which is the convergence configuration for zig-zag aggregates.

2. Scale bundles

The interspersed and external parallel shifts between the chains in the aggregates are defined by considering positive and negative
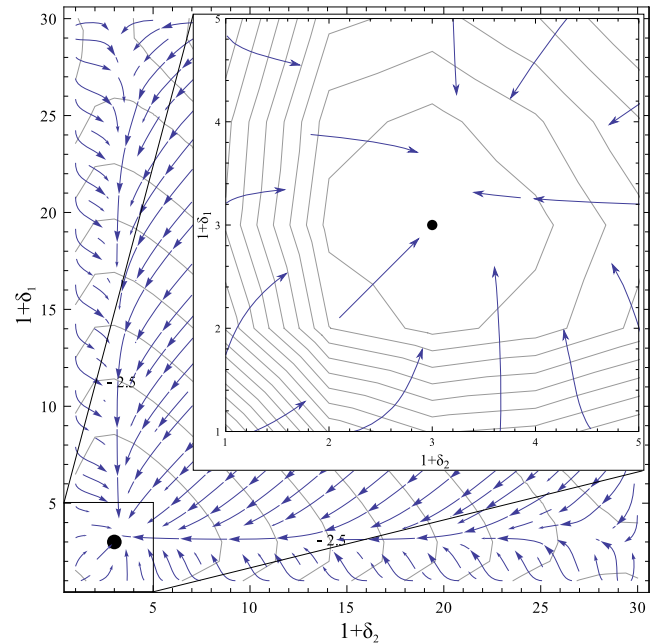
consecutive displacements δ_i; then, $\delta_{i,i+2} = \delta_i + \delta_{i+1} + 1$ (with $i = 1, 2$) and $\delta_{1,4} = \delta_1 + \delta_2 + \delta_3 + 1$ for interspersed and lateral cases, respectively, and these are general rules that apply for regular and irregular bundles (see also Sec. III). At $n = 6$, the minima of the normalized cohesion energy per particle U_4^{sca} are found at $(\delta_1, \delta_2, \delta_3) = (2, 3, 2)$ and $(\delta_1, \delta_2, \delta_3) = (-3, -4, -3)$. For $n = 10$, these minima are encountered at $(\delta_1, \delta_2, \delta_3) = (2, 6, 2)$ and $(\delta_1, \delta_2, \delta_3) = (-3, -7, -3)$. For $n = 25$, the most probable configurations are $(\delta_1, \delta_2, \delta_3) = (-3, -3, -3)$ and $(\delta_1, \delta_2, \delta_3) = (2, 2, 2)$ [see Fig. 5(c)] being also associated with the minima of U_4^{sca} at higher n. The latter arrangements are relative to the global minima of U_4 (see Table II).

3. Hill/valley aggregates

Four configurations are considered in this section (see Table I), for instance, consecutive lateral displacements in hill-1 aggregates with $\delta_1 \geq 0$, $\delta_2 \geq 0$, and $\delta_3 < 0$. Interspersed and external parallel shifts are $\delta_{i,i+2} = \delta_i + \delta_{i+1} + 1$ and $\delta_{1,4} = \delta_1 + \delta_2 + \delta_3 + 1$, following general rules. At $n = 6$, the minima of the normalized cohesion energy per particle U_4^{hil} are found at $(\delta_1, \delta_2, \delta_3) = (1, 5, -2)$ and $(\delta_1, \delta_2, \delta_3) = (1, -6, -2)$ and for U_4^{val} the minima of the potential are at $(\delta_1, \delta_2, \delta_3) = (-2, 5, 1)$ and $(\delta_1, \delta_2, \delta_3) = (-2, -6, 1)$ with the same cohesion energy. For $n = 10$ the minima of U_4^{hil} are found at $(\delta_1, \delta_2, \delta_3) = (1, 9, -2)$ and $(\delta_1, \delta_2, \delta_3) = (1, -10, -2)$, for U_4^{val}, the minima are encountered at $(\delta_1, \delta_2, \delta_3) = (-2, 9, 1)$ and $(\delta_1, \delta_2, \delta_3) = (-2, -10, 1)$. At $n = 25$ and higher, the most plausible configurations are $(\delta_1, \delta_2, \delta_3) = (2, 4, -2)$ and $(\delta_1, \delta_2, \delta_3) = (1, -5, -3)$ [see Fig. 5(d)], associated with the minima of U_4^{hil}. The minima of U_4^{val} are encountered at $(\delta_1, \delta_2, \delta_3) = (-2, 4, 2)$ and $(\delta_1, \delta_2, \delta_3) = (-3, -5, 1)$.
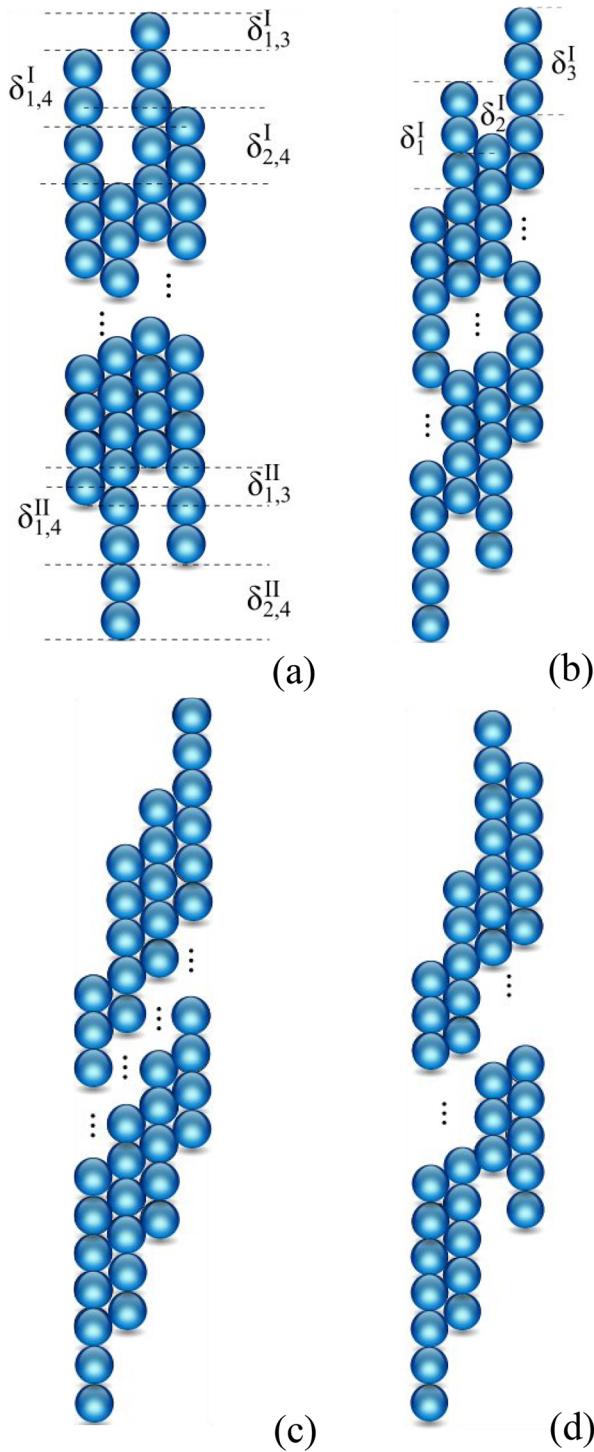

FIG. 4. Equipotentials of total reduced energy $U_3^{sca(1)}$ and force field $\vec{F}_3^{sca(1)}$ of three assembled chains for scale-1 aggregates at $n = 30$.

FIG. 5. (a) Scheme of a 4-chain zig-zag-2 aggregate with interspersed and external parallel displacements $\delta_{i,j}^l$, (b) the 4-chain zig-zag-1 bundle relative to the convergence minimum of $U_4^{zig(1)}$ at $n \gg d$ scheming consecutive parallel displacements δ_i^I, (c) the minimum energy arrangement for scale-1 aggregates as n increases, and (d) the hill-1 bundle associated with the minimum of $U_4^{hil(1)}$ as $n \to \infty$.

Reflections and 180° rotations change the category of a hill or valley ribbon, for instance, hill-1 bundles become valley-1 under reflections at the symmetry axis perpendicular to $\vec{B}$ or valley-2 agglomerates under 180° rotations having the same energy.

4. Discussion

Comparing the magnitudes of the cohesion magnetic energy of the aggregates at $d = 4$ (see Table II), the most plausible arrangements correspond to the scale configurations $(\delta_1, \delta_2, \delta_3) = (-3, -3, -3)$ and $(\delta_1, \delta_2, \delta_3) = (2, 2, 2)$ as n increases, relative to the global minima of U_4. In order to verify that these are the ground states of a 4-chain bundle, the cohesion potential differences ΔU_{4i}^{sca} are computed similarly as in Sec. II A 1,

$$\Delta U_{41}^{sca} = U_4^{sca}(\delta_1, \delta_2, \delta_3) - U_4^{sca}(\delta_1 - 1, \delta_2, \delta_3)$$
$$\Delta U_{42}^{sca} = U_4^{sca}(\delta_1, \delta_2, \delta_3) - U_4^{sca}(\delta_1, \delta_2 - 1, \delta_3)$$
$$\Delta U_{43}^{sca} = U_4^{sca}(\delta_1, \delta_2, \delta_3) - U_4^{sca}(\delta_1, \delta_2, \delta_3 - 1),$$

and the magnetic forces per particle in the aggregate $\vec{F}_4^{sca} = -\nabla U_4^{sca}$ are

$$\vec{F}_4^{sca} = -(\Delta U_{41}^{sca}\hat{\delta}_1 + \Delta U_{42}^{sca}\hat{\delta}_2 + \Delta U_{43}^{sca}\hat{\delta}_3), \qquad (7)$$

in each coordinate parallel to the magnetic field. These are the effective forces at each junction, considering the interaction between interspersed and external chains as well.

The sphere shown in Fig. 6 indicates the integer position $(\delta_1, \delta_2, \delta_3) = (2, 2, 2)$ relative to the minimum of the magnetic potential at $n = 30$, which is encountered at $U_{4i}^{sca(1)} < 0$. Notice in Fig. 6 that an integer shift in the positive (negative) direction of δ_i results in $F_{4i}^{sca(1)} < 0$ ($F_{4i}^{sca(1)} > 0$), i.e., the minimum is stable in δ_1, δ_2, and δ_3. Computation of the minima for a higher number of particles can be achieved with the present method. The minimum of $U_4^{sca(1)}$ is
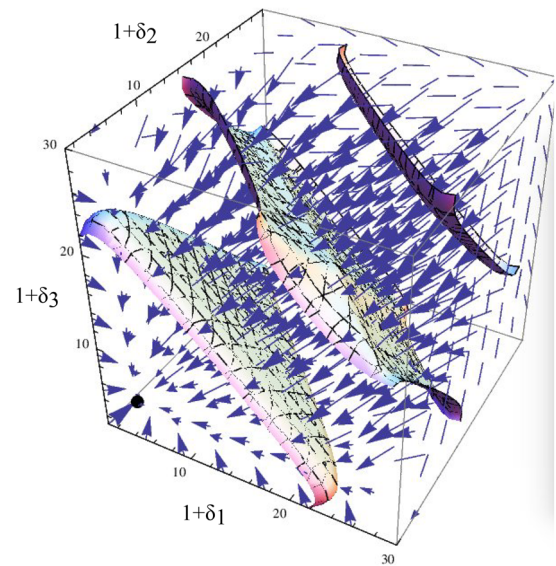

FIG. 6. Equipotentials of total reduced energy $U_4^{sca(1)}$ and force field $\vec{F}_4^{sca(1)}$ of four assembled chains for scale-1 aggregates at $n = 30$.

found at real coordinates, with $(\delta_1, \delta_2, \delta_3) = (2, 2, 2)$ being the nearest integer position. This is not the exact position of the minimum of $U_4^{sca(1)}$, and the aggregates remain in this configuration due to contact forces. In terms of the cohesive forces $\vec{F}_{4i}^{sca(1)}$ in the coordinates parallel to the magnetic field at each junction, these are weakly repulsive at $(\delta_1, \delta_2, \delta_3) = (2, 2, 2)$ and attractive toward this point at any other integer position as $n \rightarrow \infty$.

III. UNLIKE SIZED CHAINS

In this section, unlike $(n_1 \neq n_2 \neq n_3)$ sized chains (irregular ribbons) are considered to search for the most plausible configuration in aggregates of width $d = 2, 3, 4$. For these aggregates, the consecutive parallel displacements in regions I and II are different, $\delta_i^I \neq \delta_i^{II}$, (see Figs. 7 and 9). Only consecutive shifts in region I are employed $(\delta_i^I \equiv \delta_i)$. Since it was obtained for like sized chains that the magnitude of the cohesion energy in scale aggregates is higher than that of zig-zag and hill/valley cases (see Table II), only I-scaled aggregates in the positive region $(\delta_i \geq 0)$ will be studied. The total number of particles per aggregate is $n_r = \sum_{i=1}^{d} n_i$. In these cases, the dimension of the space of parameters is $\mathscr{D} = 2d - 1$, containing the length of each chain n_i and their consecutive displacements δ_i. At $d = 2$, the problem is 3-dimensional; thus, the minima of the cohesion potential are computed numerically, and its stability with respect to the lateral displacements is verified. The reduced magnetic energy of interaction[18] between 2 chains of different lengths is

$$U_{n_1,n_2}^{cc}(\delta_\parallel, \delta_\perp) = \sum_{i=1}^{n_2} \sum_{j=1}^{n_1} \left(\frac{1}{((j - i + \delta_\parallel)^2 + \delta_\perp^2)^{3/2}} - \frac{3(j - i + \delta_\parallel)^2}{((j - i + \delta_\parallel)^2 + \delta_\perp^2)^{5/2}} \right). \quad (8)$$

The cohesive energy per particle in 2-chain bundles with $n_1 \neq n_2$ (and $n_1 = n_2$) is $U_2 = (U_{n_1}^c + U_{n_2}^c + U_{n_1,n_2}^{cc}(\delta))/(n_1 + n_2)$. Formulas
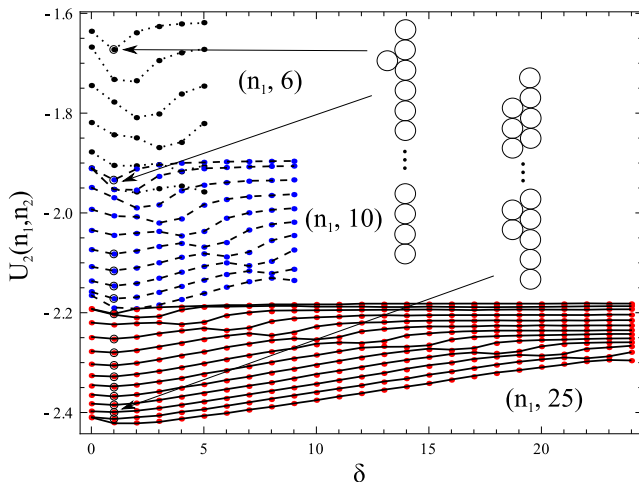

FIG. 7. Cohesion energy U_2 of two assembled chains at $n_{max} = 6$ (dotted), $n_{max} = 10$ (dashed), and $n_{max} = 25$ (continuous) curves. Schemes of aggregates $(n_1, n_2) = (1, n_2)$ and $(n_1, n_2) = (21, 25)$ at parallel displacement $\delta = 1$.

(3) and (4) are similar in these cases, specified for 3- and 4-chain irregular ribbons, respectively, as follows:

$$U_3(n_i, \delta_{i,j}) = \frac{1}{\sum_{i=1}^{3} n_i} \left(\sum_{i=1}^{3} U_{n_i}^c + \sum_{i=1}^{2} U_{n_i,n_{i+1}}^{cc}(\delta_{i,i+1}) + U_{n_1,n_3}^{int}(\delta_{1,3}) \right), \quad (9)$$

$$U_4(n_i, \delta_{i,j}) = \frac{1}{\sum_{i=1}^{4} n_i} \left(\sum_{i=1}^{4} U_{n_i}^c + \sum_{i=1}^{3} U_{n_i,n_{i+1}}^{cc}(\delta_{i,i+1}) \right.$$
$$\left. + \sum_{i=1}^{2} U_{n_i,n_{i+2}}^{int}(\delta_{i,i+2}) + U_{n_1,n_4}^{ext}(\delta_{1,4}) \right). \quad (10)$$

It will be shown in Secs. III B and III C that U_3 and U_4 depend only on the lateral displacements between consecutive chains. n_{max} is the maximum length of a chain allowed in a bundle. Aggregates aligning parallel to the magnetic field hold the condition $n_{max} \geq d$, for instance, at $d = 2$, there is one scale case in the region $\delta > 0$ that do not represent a physical assembly in the suspension (see examples in Fig. 1). The schemed trimer at $d = 2$ is an irregular bundle that can be observed with small probability, and the latter occurs when the third bead has more kinetic energy than the potential barrier of the dimer aligned parallel to the magnetic field.[18] The ratio between these nonphysical arrangements and the total number of cases strongly decrease as n_{max} increases, being negligible at $n_{max} \gg d$.

A. 2-chain bundles

The aggregate cohesion energy per particle is computed by employing $U_n^c = -2\sum_{i=1}^{n} \frac{n-i}{i^3}$ and (8) in U_2. The results are computed for $\delta \geq 0$ since configurations with negative values of δ are equivalent (aggregates can be rotated or reflected to the $\delta \geq 0$ region). A set of curves is found for all the pairs (n_1, n_2) comprising 2-chain bundles with constant n_2, variable n_1, and $n_1 \leq n_2$. In some cases two minima are found per curve, and different sets of curves intersect. Importantly, the minimum of each curve per set is mostly found at $\delta = 1$ (see rings in Fig. 7), and this minimum is encountered at $\delta = 2$ for $n_1 = n_2$ and other cases.

The number of cases $\delta = 1$ increases as $n_2 \rightarrow \infty$, and at $n_2 = 25$, only curves with odd n_1 are schemed; in this case, there are twice the number of rings than presented, more than the 70% of the minima of that set (continuous curves). Then, although the minimum of U_2 for each set is found at $\delta = 2$, when $n_1 = n_2$, for most of the combinations (n_1, n_2), the relative parallel displacement is likely to occur at $\delta = 1$ in the region $\delta \geq 0$. To confirm the latter, the ratio between the number of stable minima for each δ and the total number of chain length combinations n_{max}^2 in irregular bundles is computed with

$$r_2(\delta') = \frac{1}{n_{max}^2} \sum_{n_1=1}^{n_{max}} \sum_{n_2=1}^{n_{max}} \begin{cases} 1 & \text{if} & * \\ 0 & \text{otherwise,} \end{cases} \quad (11)$$

with $* = $ minimum of $U_2(n_1, n_2, \delta)$ is found at $\delta = \delta'$. Then, $\sum_{\delta=0}^{n_{max}-1} r_2(\delta) = 1$. Equation (11) is the probability of two interacting chains assembled in a δ' configuration, which is averaged over the total number of possible interactions. Note that the statistics are computed including aggregates formed by like sized chains ($n_1 = n_2$). At $n_{max} = 10$, U_2 minimum is mostly found at $\delta = 1$ with more than 25% of the total number of combinations (n_1, n_2). This percentage

increases as $n_{max} \to \infty$, and at $n_{max} = 35$, it is found with 44.7% of the total number of possible arrangements. The equivalent scale-2 minimum is found at $\delta = -2$.

B. 3-chain scale ribbons

Irregular aggregates of width $d = 3$ need not necessarily belong to the same category under rotations in $180°$ and reflections with the axis of symmetry perpendicular or parallel to $\vec{B}$, for instance, an I-scaled bundle under perpendicular reflection can be an I-zig-zag ribbon, having the same cohesive energy. By scheming a 3-chain irregular aggregate, it is shown that the parallel displacement between the external (interspersed in this case) chains $\delta_{1,3} = \delta_1 + \delta_2 + 1$ is independent of the number of particles of each chain n_i with $i = 1, 2, 3$. It is recalled that $\delta_1 \leq n_2 - 1$ and $\delta_2 \leq n_3 - 1$; otherwise, (n_1, n_2, n_3) does not represent assembled chains. Three scale-1 cases are noted: $(n_1, n_2) \leq n_3$, $(n_1, n_3) \leq n_2$, and $(n_2, n_3) \leq n_1$, see Fig. 9.

The cohesion energy of irregular bundles is computed by employing Eq. (9). In order to find the minima of the cohesive energy of 3 assembled chains, the potential differences $\Delta U_{3i}^{sca}(n_1, n_2, n_3)$ are computed similar to that performed in Sec. II A 1,

$$\Delta U_{31}^{sca} = \left(U_3^{sca}(\delta_1, \delta_2) - U_3^{sca}(\delta_1 - 1, \delta_2) \right)\big|_{n_1, n_2, n_3},$$

$$\Delta U_{32}^{sca} = \left(U_3^{sca}(\delta_1, \delta_2) - U_3^{sca}(\delta_1, \delta_2 - 1) \right)\big|_{n_1, n_2, n_3}.$$

Each difference is computed considering constant n_i and $i = 1, 2, 3$. The magnetic forces per particle $\vec{F}_3^{sca}(n_1, n_2, n_3) = -\nabla U_3^{sca}$ in the aggregate are

$$\vec{F}_3^{sca}(n_1, n_2, n_3) = -\left(\Delta U_{31}^{sca}\hat{\delta}_1 + \Delta U_{32}^{sca}\hat{\delta}_2 \right)\big|_{n_1, n_2, n_3}. \quad (12)$$

Figure 8 show an example of the equipotentials of the cohesive energy and the force field of a scale-1 aggregate $(n_1, n_2, n_3) = (20, 15, 10)$ in $(\delta_1, \delta_2) \geq 0$ space. As observed previously, a stable minimum is found at the real position near the integer position $(\delta_1, \delta_2) = (2, 2)$ (circle); thus, in this case, the chains will most likely aggregate in this configuration and remain there due to magnetic and contact forces. The minima of each surface are computed in order to obtain a ratio accounting for the type of configuration and the most plausible relative displacements of aggregates formed by three unlike sized chains. The (δ_1, δ_2) surfaces in the three cases considered in Fig. 9 are studied up to $n_{max} = 15$ for scale-1 cases, i.e., up to regular aggregates formed by three chains of length $n_{max} = 15$. At $n_{max} = 10$ (see blue surface sets), the stable assembly $(\delta_1, \delta_2) = (3, 2)$ is the most probable for any configuration $(n_1, n_2, n_3) \leq n_{max}$, with 4.2% of the total of possible combinations n_{max}^3. In general, this percentage is computed with the ratio

$$r_d(\delta_1', \ldots, \delta_{d-1}') = \frac{1}{n_{max}^d} \sum_{n_1=1}^{n_{max}} \cdots \sum_{n_d=1}^{n_{max}} \begin{cases} 1 \text{ if } \quad ** \\ 0 \text{ otherwise} \end{cases}, \quad (13)$$

with $** = $ minimum of $U_d(n_1, \ldots, n_d, \delta_1, \ldots, \delta_{d-1})$ being found at $(\delta_1, \ldots, \delta_{d-1}) = (\delta_1', \ldots, \delta_{d-1}')$ and $\sum_{\delta_1=0}^{n_{max}-1} \cdots \sum_{\delta_{d-1}=0}^{n_{max}-1} r_d = 1$. Equation (13) is the probability of d interacting chains assembled in a $(\delta_1', \ldots, \delta_{d-1}')$ configuration, which is averaged over the total number of possible chain lengths. In addition, at $d = 3$ and $n_{max} = 10$, the pair $(\delta_1, \delta_2) = (2, 2)$ is highly plausible with 4.1%, which is similar to the case presented in Fig. 8 (in that case, $n_{max} = 20$). At
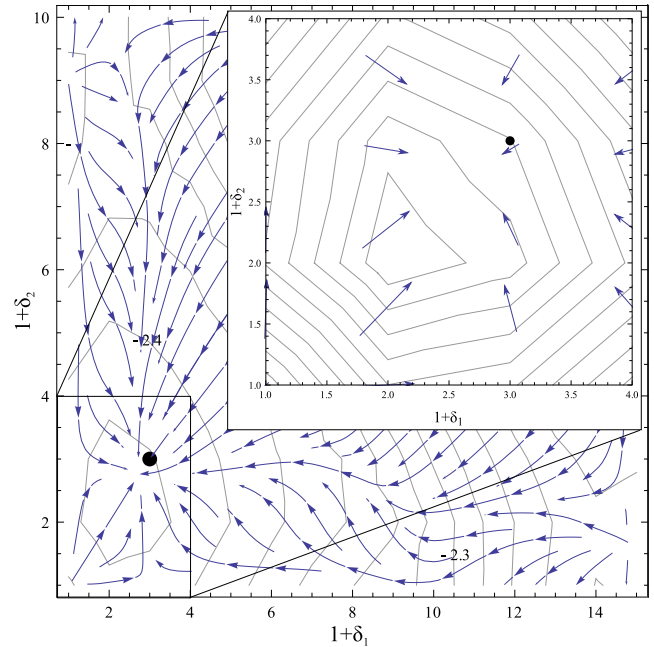

FIG. 8. Equipotentials of the cohesion energy per particle $U_3^{sca(1)}$ and force field $\vec{F}_3^{sca(1)}$ of three assembled chains at $(n_1, n_2, n_3) = (20, 15, 10)$.

$n_{max} = 12$, the configuration $(\delta_1, \delta_2) = (2, 2)$ is the most probable assembly, associated with the stable minimum of $U_3^{sca(1)}$, with more than 4.5% of the total number of arrangements. At $n_{max} = 15$, this stable minimum is observed in 5.1% of the total configurations. At $n_{max} = 16$, the minimum of the magnetic potential is found at $(\delta_1, \delta_2) = (1, 2)$, with about 5.4%, and at $n_{max} = 17$, it is found with 5.7%, increasing with n_{max} as predicted; thus, $(\delta_1, \delta_2) = (2, 2)$ up to $n_{max} = 15$ and $(\delta_1, \delta_2) = (1, 2)$ observed up to $n_{max} = 20$ are metastable minima. This has been computed at $n_{max} = 30$, and the stable minimum $(\delta_1, \delta_2) = (1, 1)$ has been found to be the most plausible, with about 7.9%. The latter finding confirms that the most probable configuration is $(\delta_1, \delta_2) = (1, 1)$ as n_{max} increases, similar to the case $d = 2$ where $\delta = 1$ is the most probable arrangement. For scale-2 ribbons, $(\delta_1, \delta_2) = (-2, -2)$ is the equivalent configuration in most of the arrangements (n_1, n_2, n_3) as $n_{max} \to \infty$. The present method can be employed to compute these statistics for zig-zag aggregates.

C. 4-chain scale aggregates

As for irregular 3-chain bundles, at $d = 4$, irregular ribbons do not necessarily belong to the same category under rotations in $180°$ and reflections at the axes of symmetry perpendicular or parallel to $\vec{B}$, having the same cohesive energy. By scheming a 4-chain irregular aggregate, it is shown that the parallel shifts between the interspersed chains $\delta_{i,i+2} = \delta_i + \delta_{i+2} + 1$ (with $i = 1, 2$) and the relative displacement between external chains $\delta_{1,4} = \delta_1 + \delta_2 + \delta_3 + 1$ are independent of the number of particles of each chain n_i with $i = 1, \ldots, 4$. The magnetic energy U_4^{sca} is not presented in this case since the
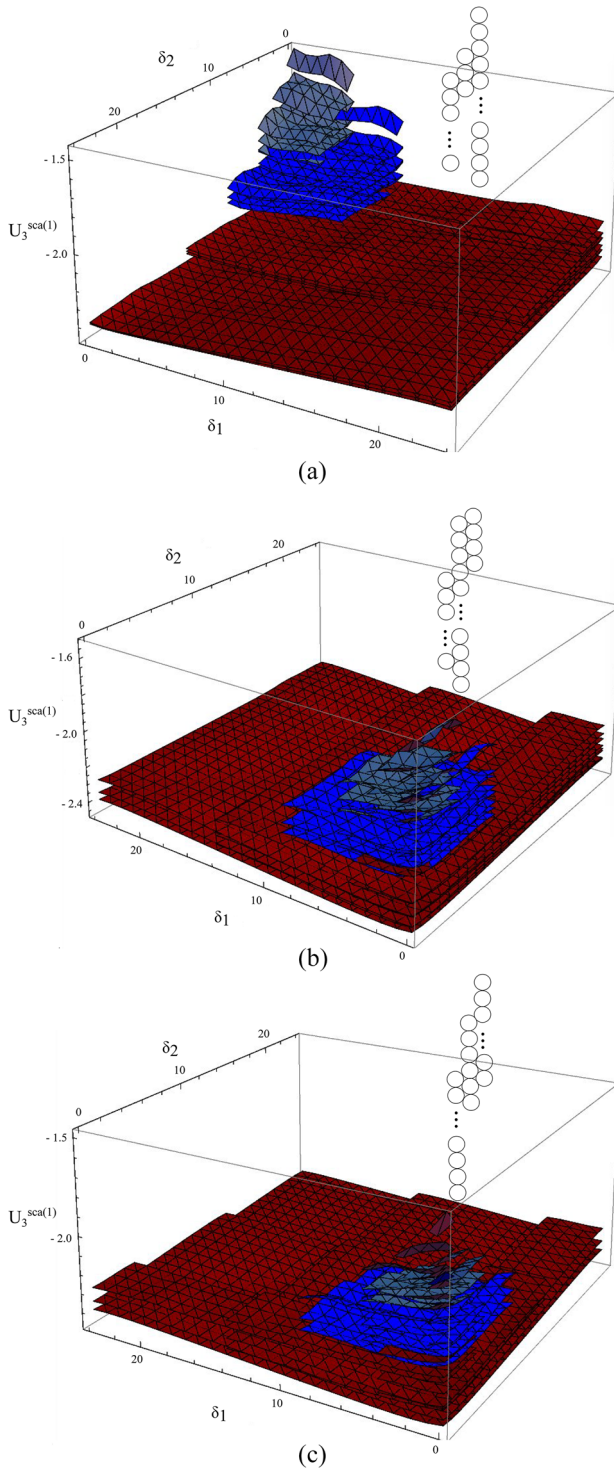
FIG. 9. Cohesion energy $U_3^{sca(1)}(n_1, n_2, n_3, \delta_1, \delta_2)$ of three assembled chains for scale-1 irregular aggregates at $n_{max} = 6$ (gray), $n_{max} = 10$ (blue), and $n_{max} = 25$ (red) surfaces in cases (a) $(n_1, n_2) \leq n_3$, (b) $(n_1, n_3) \leq n_2$, and (c) $(n_2, n_3) \leq n_1$. Inset: scale-1 irregular bundles at (a) $(n_1, 3) \leq n_3$ and $(\delta_1, \delta_2) = (1, 2)$, (b) $(n_1, 4) \leq n_2$ and $(\delta_1, \delta_2) = (3, 0)$, and (c) $(6, n_3) \leq n_1$ and $(\delta_1, \delta_2) = (3, 2)$.

parameter space is 3 dimensional in δ_i; the equipotentials of U_4^{sca} and force field $\vec{F}_4^{sca}$ are computed (as in Sec. III B) by employing

$$\Delta U_{4j}^{sca} = \left(U_4^{sca}(\dots, \delta_j, \dots) - U_4^{sca}(\dots, \delta_j - 1, \dots)\right)\big|_{n_i},$$

for each set $n_i = n_1, \dots, n_4$ and $j = 1, 2, 3$. The magnetic forces per particle $\vec{F}_4^{sca}$ are

$$\vec{F}_4^{sca}(n_i) = -\left(\Delta U_{41}^{sca}\hat{\delta}_1 + \Delta U_{42}^{sca}\hat{\delta}_2 + \Delta U_{43}^{sca}\hat{\delta}_3\right)\big|_{n_i}, \qquad (14)$$

for each junction parallel to the magnetic field. The sphere in Fig. 10 indicates the integer position relative to the stable minimum of the irregular aggregate $(n_1, n_2, n_3, n_4) = (20, 25, 30, 35)$. An integer shift in the positive (negative) direction of δ_i yields $F_{4i}^{sca(1)} < 0$ ($F_{4i}^{sca(1)} > 0$); then, the minimum is stable in δ_1, δ_2, and δ_3. The minima of $U_4^{sca(1)}$ are computed in order to obtain a ratio accounting for the most plausible relative displacements of ribbons formed by 4 unlike sized chains.

The computation is performed in parallel, employing a 4-core Intel Pentium processor; at $n_{max} > 9$, the computation time length increases from hours to days. The ratio is computed by employing (13) in the case $d = 4$. From $n_{max} = 9$ up to $n_{max} = 12$, the stable minimum $(\delta_1, \delta_2, \delta_3) = (1, 4, 2)$ is the most probable configuration with 1.02% and 0.85% (respectively) from all the possible aggregates $(n_1, n_2, n_3, n_4) \leq n_{max}$. This percentage decreases as n_{max} increases, meaning that this configuration is not the most probable as $n_{max} \to \infty$. At $n_{max} = 12$, the arrangement $(\delta_1, \delta_2, \delta_3) = (2, 2, 2)$ is at the eighth place, with 0.675% (see Fig. 10). As n_{max} increases, the computation time length increases from weeks to months. It is claimed that the positions of the minima move toward $(\delta_1, \delta_2, \delta_3) = (1, 1, 1)$ and $(\delta_1, \delta_2, \delta_3) = (-2, -2, -2)$ as $n_{max} \to \infty$, and the latter will be confirmed by employing cluster computing.
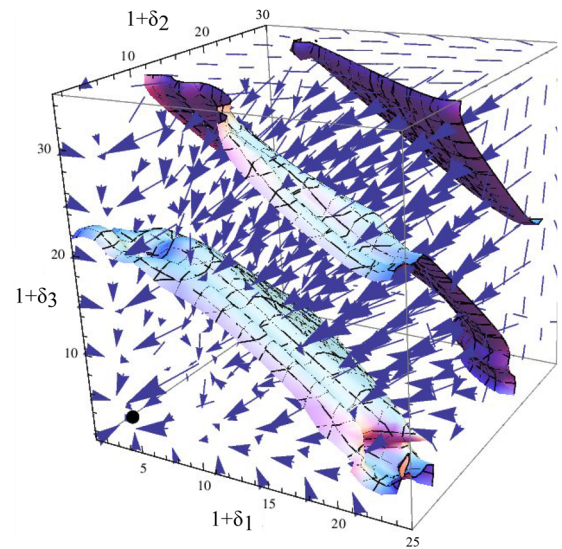

FIG. 10. Equipotentials of total reduced energy $U_4^{sca(1)}$ and force field $\vec{F}_4^{sca(1)}$ of a 4-chain scale-1 irregular aggregate at $(n_1, n_2, n_3, n_4) = (20, 25, 30, 35)$.

IV. AGGREGATE MEAN LENGTH

In this section, the mean length of regular aggregates composed of two, three, and four chains of the same length is computed, taking into account the most probable lateral displacements between consecutive chains obtained in Sec. II and the development of the equilibrium constant without approximations[20,23] at this level, although there have been approximations concerning the hydrodynamic interaction forces. The following nondimensional groups are important to distinguish between dominant and negligible forces. Particles detach fluid streamlines because they move following local magnetic field lines around the clusters; hence, the hydrodynamic Stokes number is high, $St > 1$. A low Reynolds number means viscous bulk hydrodynamic forces mostly affect the chain aggregation process. An important nondimensional group is the magnetic Peclet number. In recent studies,[16,17] researchers have shown that the Peclet number – comparing magnetic forces to the hydrodynamic drag force of the particles' random walk in the fluid – is low ($Pe < 1$) and when it is lower than the critical Peclet number $Pe_c = 0.825$, the chain growth curves can be collapsed. Then, viscous forces are comparable to magnetic forces in the chain aggregation regime, which is not the case at the ribbon aggregation and saturation phases due to higher magnetic fields. One main difference between the chain and bundle saturation regimes is that in the latter stage chains clip off bundles to interact with other ribbons, maintaining their alignment to the applied magnetic field. Thus, in this regime, $Pe > Pe_c$ since the applied magnetic field is high and magnetic forces between the aggregates are dominant over hydrodynamic forces, even at very viscous solvents. Magnetic energies per particle U_2, U_3, and U_4 in formula (9) are fitted for $d = 2, 3, 4$ at the most plausible lateral consecutive displacements in regular aggregates $\delta = 2$, $(\delta_1, \delta_2) = (2, 2)$, and $(\delta_1, \delta_2, \delta_3) = (2, 2, 2)$, respectively
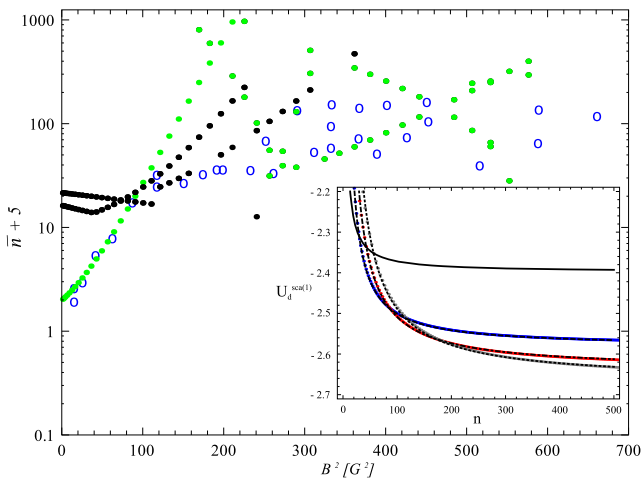

FIG. 11. Mean length of the aggregates in the colloidal suspension. Experimental data obtained from Ref. 19 (circles) are compared against the absolute value of complex (black points) and real (green/gray points) solutions of (15). Inset: magnetic cohesive energy per particle $U_2^{sca(1)}$, $U_3^{sca(1)}$, and $U_4^{sca(1)}$ of scale-1 aggregates containing like-sized chains as a function n and fit in cases $d = 1$ (continuous), $d = 2$ (dashed), $d = 3$ (dotted-dashed), and $d = 4$ (dotted).

[see Fig. 11 (inset)]. The fit coefficients (a_1, b_1) are those found in Ref. 19 in the case $d = 1$. The constants of the magnetic energy for these regular cases are $a_d = 1.3054, 4.0500, 6.4900$, and 8.9000 and $b_d = 1.1997, 1.2910, 1.3193$, and 1.3335 at $d = 1, 2, 3, 4$, respectively. Importantly, for the latter fit, the local minimum changes at about $n_d = 30, 85, 180$ at $d = 2, 3, 4$. The fit (a_d, b_d) for the magnetic energy is used in the computation of the Boltzmann factor $r_{d,n}$ and the equilibrium constant $K_{d,n}$, employing the average length of the chains in the agglomerates,

$$\bar{n} = \frac{1}{A} \sum_{d=1}^{4} \sum_{n=d}^{\infty} n A_{d,n}, \tag{15}$$

with $A = \sum_{d=1}^{4} \sum_{n=d}^{\infty} A_{d,n}$ bring the total number of bundles in the fluid and $A_{d,n} = \phi_{d,n}/dnV_\odot$ the number of aggregates of width d and chains of length n in scale, zig-zag, or hill/valley configurations. The volume fraction $\phi_{d,n} = dnx^{dn}\phi_{1,1}r_{d,n}K_{d,n}/x$ (see details in Ref. 19) is written as a function of $x = \phi_{1,1}e^{\beta\varepsilon_m}$ with $\phi_{1,1}$ being the volume fraction of monomers under magnetic field applied and $\beta = 1/k_BT$ with T the suspension mean temperature. $K_{d,n} = (\bar{n}_r/\phi_0)^{dn-1}$ is the equilibrium constant, $\bar{n}_r$ the average number of beads per ribbon, and $\phi_0 = NV_\odot/V$ is the volume fraction of monomers in absence of a magnetic field. The factor $r_{d,n} = e^{\beta\varepsilon_m[1-a_d+(b_d-1)dn]}$ depends on the cohesive magnetic energy per particle of the bundles. It is noted that (15) is the mean length of the bundles in cases where the lateral displacement between chains is small (the aggregates are roughly rectangular). This is also the case of the configurations found in Sec. II, where Eq. (15) differs on a factor of order $2.5(d - 1) < 10$ compared upon the length of the most plausible scale agglomerates; thus, $\bar{n} + 5$ is computed in the bundle regime $d = 2, 3, 4$. Complex and real solutions are obtained by solving the set (i) $\bar{n}_r = x_0/a_0$, (ii) $\bar{n} = n_0/a_0$, (iii) $x_0 = \sum_{d=1}^{4} x_{0d}$ for $(x, \bar{n}_r, \bar{n})$, with $a_0 = \sum_{d=1}^{4} a_{0d}$, $n_0 = \sum_{d=1}^{4} n_{0d}$, and

$$\begin{aligned} a_{0d} &= \frac{\phi_0}{\bar{n}_r} e^{\beta\varepsilon_m(1-a_d)} \frac{\zeta_d^{d^2}}{1-\zeta_d^d}, \\ n_{0d} &= a_{0d}\left(d + \frac{\zeta_d^{d^2}}{1-\zeta_d^d}\right), \end{aligned} \tag{16}$$

$x_{0d} = dn_{0d}$ and $\zeta_d = (\bar{n}_r/\phi_0)xe^{\beta\varepsilon_m(b_d-1)}$. These equations have a maximum of 20 complex and pure real solutions from which 4 real (green/gray points) and complex (black points) solutions are selected (see Fig. 11). The solutions of $\bar{n}$ are plotted for values of B in the range [1, 26] G at $\phi_0 = 0.003$ and $C_1 = 0.25 \times 10^{-2}$ $[G^{-2}]$ (points) in good agreement with experimental measurements (circles). Numerical results can be easily modified by tuning ϕ_0 and C_1. Multistability is observed in the ribbons regime $B^2 \gtrsim 300$ $[G^2]$. In the chain range ($d = 1$) the set (i)–(iii) is undetermined due to $\bar{n}_r = \bar{n}$, the numerical solutions are obtained solving (ii) and (iii) for the variables x and $\bar{n}$ with parameters $\phi_0 = 0.003$ and $C_1 = 2.5 \times 10^{-2}[G^{-2}]$ (points). The employed values of C_1 at each regime differ by one order of magnitude due to the minimum and maximum values of the experimental measurements of χ and R. The solutions of the set (ii) and (iii) are real with maximum multiplicity equal to 1 in this range of parameters.

For aggregates with unlike-sized chains, magnetic energy can be fitted at $d = 2, 3, 4$ for the most plausible lateral consecutive

displacements $\delta = 1$, $(\delta_1, \delta_2) = (1, 1)$, and $(\delta_1, \delta_2, \delta_3) = (1, 1, 1)$, respectively. Nevertheless, the number of beads in each chain is arbitrary; thus, any set $(n_1, \ldots, n_d)$ can be chosen. In this case, the results obtained in Sec. III are useful if the number of particles of each chain per interaction is known. The theoretical findings are more scattered than experimental data at values of B^2 higher than about 150 $[G^2]$ and lower than 300 $[G^2]$. This discrepancy is due to many factors including sedimentation, inter-particle hydrodynamic and contact forces (e.g., lubrication and Hertz forces), and due to the statistical mean calculation considering the selected scale ribbon configurations. It is noted that these configurations represent a large amount of bundles since their fraction in the suspension grows as increasing the allowed maximum number of particles per chain; nevertheless, there are bundle arrangements that are not considered in the ribbon average length computation. Also, the range of B^2 previously commented belongs to chain formation and saturation regimes where viscous forces are important, $Pe < Pe_c$; then, a discrepancy in this range is expected.

V. CONCLUSIONS

In this work, ribbons formed by like sized and unlike sized chains at consecutive lateral displacements δ_i were studied. In Sec. II, regular scale aggregates are found to be the most energetic at d = 2, 3, 4, and this is used to guide the study at irregular bundles (Sec. III). In Sec. II A, the first numerical results confirm that $\delta = -3$ and $\delta = 2$ are associated with the minima of the cohesive energy of a 2-chain regular aggregate. 3-chain bundles are classified in zigzag and scale types. The stability of the minima is studied in the $(\delta_1, \ldots, \delta_{d-1})$ parameter space. The findings predict stable global minima around the integer positions $(\delta_1, \delta_2) = (-3, -3)$ and (δ_1, δ_2) = (2, 2) as n increases. In Sec. II B, 4-chain aggregates are classified in zig-zag, scale and hill/valley cases. The minima of U_4^{sca} are found around the integer positions $(\delta_1, \delta_2, \delta_3) = (-3, -3, -3)$ and $(\delta_1, \delta_2, \delta_3) = (2, 2, 2)$ as $n \to \infty$, these are the positions associated with the global minima of the cohesive energy U_4 for any type of bundle composed by 4 chains of equal length. For instance, at $d = 3$, a chain joins a pair of assembled chains similar to the assembly of a single chain. At $d = 4$, a chain will most likely join a 3-chain regular bundle to build a 4-chain regular ribbon at these most probable configurations. The chain aggregation process can be also performed by pairs in the case $d = 4$. The aggregates remain in the integer positions due to contact forces and depletion zones. Section III considers irregular ribbons formed by unlike sized chains. The ratio between the number of configurations $(\delta_1, \ldots, \delta_{d-1})$ (where the minima of U_d are encountered) and the total number of possible aggregates $(n_1, \ldots, n_d)$ is computed in order to define the most common assembly per bundle width. In Sec. III A, considering the case of two assembled chains (d = 2) and $n_{max} = 35$, more than the 44% of the possible assemblies have a minimum of the cohesive energy at $\delta = 1$, and this percentage increases as $n_{max} \to \infty$. Then, it is more likely to form a $\delta = 1$ configuration since the $\delta = 2$ assembly occur in particular cases, for instance, when 2 chains of equal length interact. In Sec. III B, at $d = 3$ and up to $n_{max} = 15$, the pair $(\delta_1, \delta_2) = (2, 2)$ is the most plausible to be found at about 5% of the total configurations. This is a metastable minimum, and at $n_{max} = 17$, the minimum of the magnetic potential is found at $(\delta_1, \delta_2) = (1, 2)$ with about a 5.7% increase with n_{max}. At $n_{max} = 30$, the stable minimum $(\delta_1, \delta_2) = (1, 1)$ is the most probable with about

7.9%. The latter confirms that $(\delta_1, \delta_2) = (1, 2)$ is a transitional state and the configuration $(\delta_1, \delta_2) = (1, 1)$ is the most probable to observe at unlike sized chains assemblies as n_{max} increases. In Sec. III C, at $d = 4$, the computation length increases from weeks to months at $n_{max} \geq 15$ with a 4-core Intel Pentium processor running in parallel. Based on the probabilities computed up to $n_{max} = 12$ and the results obtained in Secs. III B and III C, it is claimed that $(\delta_1, \delta_2, \delta_3) = (-2, -2, -2)$ and $(\delta_1, \delta_2, \delta_3) = (1, 1, 1)$ are the most plausible configurations as n_{max} increases, and the latter will be confirmed by employing cluster computing. It can be concluded that for regular and irregular bundles, the arrangements $\delta = -2$ and $\delta = 1$ at $d = 2$, $(\delta_1, \delta_2) = (-2, -2)$ and $(\delta_1, \delta_2) = (1, 1)$ at $d = 3$, and $(\delta_1, \delta_2, \delta_3)$ = $(-2, -2, -2)$ and $(\delta_1, \delta_2, \delta_3) = (1, 1, 1)$ at $d = 4$ are the most likely to occur in the colloidal suspension. These statistics are useful, for instance, to establish plausible assumptions for computing and fit the normalized magnetic energy per particle U_d in regular agglomerates as a function of their number of beads, which is employed to predict the mean length of the bundles in the liquid as a function of the magnetic field (see Sec. IV). The arbitrariness on the parallel shifts in irregular ribbons considered to compute and fit U_d for each case $d = 2$, 3, 4 is solved by employing the highest ratio 12 related to the probability that d interacting chains assembled in a $(\delta_1', \ldots, \delta_{d-1}')$ configuration. The findings in this work can be used also as additional constraints relative to the interaction between chains in numerical simulations.

DATA AVAILABILITY

The data that support the findings of this study are available from the corresponding author upon reasonable request.

REFERENCES

[1] A. Hütten, D. Sudfeld, I. Ennen, G. Reiss, K. Wojczykowski, and P. Jutzi, "Ferromagnetic FeCo nanoparticles for biotechnology," J. Magn. Magn. Mater. **293**, 93–101 (2005).

[2] J. K. Lim, D. C. J. Chieh, S. A. Jalak, P. Y. Toh, N. H. M. Yasin, B. W. Ng, and A. L. Ahmad, "Rapid magnetophoretic separation of microalgae," Small **8**, 1683–1692 (2012).

[3] A. Munaz, M. J. A. Shiddiky, and N.-T. Nguyen, "Recent advances and current challenges in magnetophoresis based micro magnetofluidics," Biomicrofluidics **12**, 031501 (2018).

[4] J. M. Tavares, J. J. Weis, and M. M. Telo da Gama, "Strongly dipolar fluids at low densities compared to living polymers," Phys. Rev. E **59**, 4388–4395 (1999).

[5] A. Darras, J. Fiscina, M. Pakpour, N. Vandewalle, and G. Lumay, "Ribbons of superparamagnetic colloids in magnetic field," Eur. Phys. J. E **39**, 47 (2016).

[6] C. Kittel, *Introduction to Solid State Physics*, 8th ed. (John Wiley & Sons, Inc., 2005).

[7] J. Faraudo, J. S. Andreu, and J. Camacho, "Understanding diluted dispersions of superparamagnetic particles under strong magnetic fields: A review of concepts, theory and simulations," Soft Matter **9**, 6654–6664 (2013).

[8] S. S. Leong, Z. Ahmad, and J. Lim, "Magnetophoresis of superparamagnetic nanoparticle at low field gradient: Hydrodynamic effect," Soft Matter **11**, 6968–6980 (2015).

[9] S. S. Leong, Z. Ahmad, J. Camacho, J. Faraudo, and J. Lim, "Kinetics of low field gradient magnetophoresis in the presence of magnetically induced convection," J. Phys. Chem. C **121**(9), 5389–5407 (2017).

[10] M. Fratzl, S. Delshadi, T. Devillers, F. Bruckert, O. Cugat, N. M. Dempsey, and G. Blaire, "Magnetophoretic induced convective capture of highly diffusive superparamagnetic nanoparticles," Soft Matter **14**, 2671–2681 (2018).

[11] M. Kolb, "Unified description of static and dynamic scaling for kinetic cluster formation," Phys. Rev. Lett. **53**, 1653–1656 (1984).

[12] S. Miyazima, P. Meakin, and F. Family, "Aggregation of oriented anisotropic particles," Phys. Rev. A **36**, 1421–1427 (1987).

[13] S. Fraden, A. Hurd, and R. Meyer, "Electric-field-induced association of colloidal particles," Phys. Rev. Lett. **63**, 2373–2376 (1989).

[14] J. H. E. Promislow, A. P. Gast, and M. J. Fermigier, "Aggregation kinetics of paramagnetic colloidal particles," J. Chem. Phys. **102**, 5492 (1998).

[15] F. Martínez-Pedrero, M. Tirado-Miranda, A. Schmitt, and J. Callejas-Fernández, "Formation of magnetic filaments: A kinetic study," Phys. Rev. E **76**, 011405 (2007).

[16] A. Darras, E. Opsomer, N. Vandewalle, and G. Lumay, "Superparamagnetic colloids in viscous fluids," Sci. Rep. **7**, 1–8 (2017).

[17] A. Darras, E. Opsomer, N. Vandewalle, and G. Lumay, "Effect of volume fraction on chains of superparamagnetic colloids at equilibrium," Eur. Phys. J. E **42**, 1–9 (2019).

[18] R. Messina and I. Stanković, "Self-assembly of magnetic spheres in strong homogeneous magnetic field," Physica A **466**, 10–20 (2017).

[19] N. Rojas, A. Darras, and G. Lumay, "Self-assembly processes of superparamagnetic colloids in a quasi-two-dimensional system," Phys. Rev. E **96**, 012608 (2017).

[20] N. Rojas, "Self-organization and energy of superparamagnetic nets," Phys. Rev. E **99**, 042606 (2019).

[21] J. Faraudo, J. S. Andreu, C. Calero, and J. Camacho, "Predicting the self-assembly of superparamagnetic colloids under magnetic fields," Soft Matter **26**, 3837–3858 (2016).

[22] R. Messina and L. Spiteri, "On the interaction of dipolar filaments," Eur. Phys. J. E **39**, 81 (2016).

[23] N. J. Israelachvili, "Thermodynamic principles of self-assembly," in *Intermolecular and Surface Forces*, 2nd ed. (Academic Press, 1992), pp. 341–350.